Radio Frequency Interference Pattern Detection from Sentinel-1 SAR Data Using U-NET-Like Convolutional Neural Network

3 authors:

Ojasvi Saini
Indian institute of remote sensing
17 PUBLICATIONS   38 CITATIONS

SEE PROFILE

Ashutosh Bhardwaj
Indian Space Research Organization
142 PUBLICATIONS   602 CITATIONS

SEE PROFILE

Rajat Subhra Chatterjee
Indian Institute of Remote Sensing
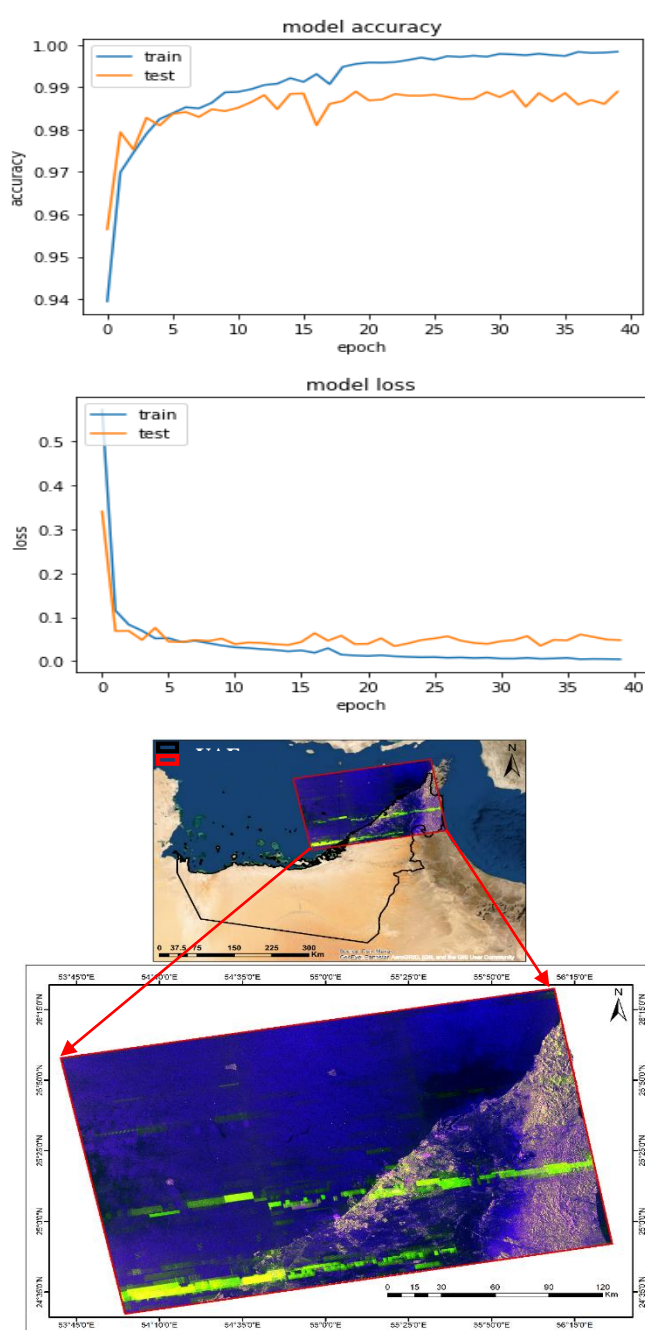111 PUBLICATIONS   1,165 CITATIONS

SEE PROFILE

Radio Frequency Interference Pattern Detection from Sentinel-1 SAR Data Using U-NET-Like Convolutional Neural Network

Ojasvi Saini [a], Ashutosh Bhardwaj [a], R.S. Chatterjee [a]

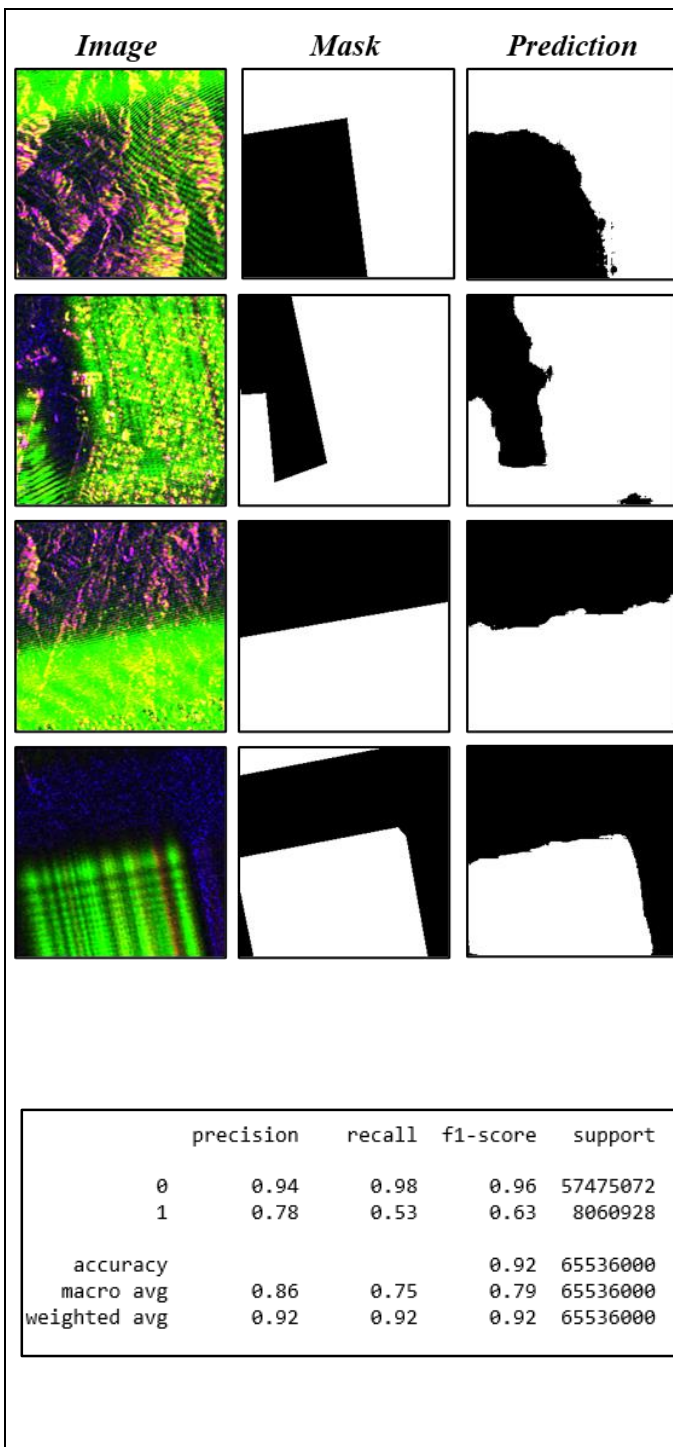*[a] Indian Institute of Remote Sensing (IIRS), Dehradun*

(*ojasvi@iirs.gov.in, ashutosh@iirs.gov.in, rschatterjee@iirs.gov.in*)

Graphical Abstract

Abstract.

Synthetic Aperture Radar (SAR) remote sensing plays an important role in several research areas such as forest conservation, crop monitoring, land hazards monitoring, elevation product generation, and strategic applications. SAR has active imaging capability with an ability to discriminate terrain features, along with recognition of selected natural as well as man-made targets. However, the special abilities of SAR become ineffective in specific cases due to interference of SAR frequency bands with the same magnitude range of radio frequencies originating from other types of electronic equipment. These types of equipment may include air-traffic surveillance radars, meteorological radars, communication systems, Radio Local Area Network (RLAN), and other electromagnetic (EM) radiation sources. The process of SAR frequency band contamination with other operating radio frequencies used for various purposes is called Radio Frequency Interference (RFI). Due to the increasing communication applications based on EM radiation, a wide range of EM spectrum is being used for this purpose. SAR frequency bands are very closely packed and even overlapping with other's operating frequency bands allotted for other applications. Due to gaps in the unified international planning for EM spectrum band allocation for different applications, the problem

	precision	recall	f1-score	support
0	0.94	0.98	0.96	57475072
1	0.78	0.53	0.63	8060928
accuracy			0.92	65536000
macro avg	0.86	0.75	0.79	65536000
weighted avg	0.92	0.92	0.92	65536000

of RFI is rapidly rising in every communication application. The satellites of the Sentinel-1 constellation use a radar, which operates in the IEEE (Institute of Electrical and Electronics Engineers) standard defined C band (central frequency 5.405 GHz) covering most civilian use frequencies. The RFIs discussed in the study manifest themselves on Sentinel-1 data in the form of lines having bright signatures, which are always perpendicular to the satellite orbit trajectory. These patterns may be hundreds of kilometres long and signify that a powerful radio source close to 5.405 GHz (such as some radars) is active and emitting somewhere along those lines. These interference patterns rigorously reduce the SAR image quality, which results in reducing the usefulness of SAR images, especially for high-resolution data-based applications. Therefore, an effective RFI pattern detection method is necessary for prior identification of RFI contaminated SAR images. In this study, openly accessible Sentinel-1 dual polarimetric (GRD) SAR image taken over busy maritime shipping port having international trade such as in Dubai has been used for the semantic segmentation of RFI patterns. The RGB composite image of the experimental site has been used to test and train the U-Net-like architecture of Convolutional Neural Network (CNN) for RFI pattern recognition.

Introduction

SAR is a leading technology on various fronts of land and ocean applications with the capabilities of, all-weather, full-time, long-range, wide-swath, and high-resolution imaging [1][2][3][4][5]. SAR has established itself to be a very important, effective, and efficient technique in the field of remote sensing [6]. It is found to be potentially competent for various land and ocean applications. Detection and characterization of natural and anthropogenic oil seepages [7], ship detection and monitoring [8][9], analysis of ocean current[10], and ocean ice monitoring [11] are some of the widely employed ocean applications using SAR remote sensing [12]. Whereas, forest monitoring [13], land use land cover mapping [14], crop monitoring [15], geomorphological analysis of ground features [16], flood

monitoring [17], digital elevation model generation [18], land deformation [19] (caused by earthquakes, landslides, or glacier advancement) are the examples the land applications that are employed using SAR technology.

Nowadays, RFI is a rapidly emerging challenge in the field of imaging radar, since more and more wireless electronic systems share the frequency spectrum for various kinds of applications [20]. Air-traffic surveillance radars, meteorological radars, communication systems, Radio Local Area Network (RLAN), and other EM radiation sources interfere with the SAR signal if the frequency spectrum of these systems overlaps with the frequency spectrum of the SAR system [21]. RFI is a serious cause of the SAR image quality degradation and it is primarily responsible for the corrupted information of ground targets, misinterpretation of the scattering properties, and inaccurate feature extraction [22]. The presence of strong RFI would yield inaccurate estimates of critical Doppler parameters (e.g., centroid and modulation rate), which would result in blurry and defocused SAR images [23]. The presence of the haze-like RFI in SAR images leads to the misinterpretation of interesting targets.

Advanced SAR systems, such as DLR's Tandem-L mission, NASA's EcoSAR and DBSAR are capable of suppressing the RFI on board or in post-processing by utilizing the Digital Beamforming (DBF) [20], but the previously launched operating SAR satellite missions such as Sentinel-1 and RadarSAT-2 are facing the problem of RFI.

The Sentinel-1 constellation SAR satellites use a radar that operates on a central frequency of 5.405 GHz and is defined as C-band by the Institute of Electrical and Electronics Engineers (IEEE) [24]. Based on power and relative distance, radio sources and receivers (used for different kinds of applications) can affect each other's performance if they operate on similar frequencies. The appearance of typical interference lines in the Sentinel-1 data images is a consequence of the interference between the SAR wave and powerful radio emitters which are operating on a frequency close to 5.405 GHz. The RFI patterns discussed in the study manifest themselves in the imagery in the form of lines with bright signature and which are always perpendicular to the satellite orbit trajectory. These patterns can be hundreds of kilometres long which signify that any powerful radio source (such as some radars) which is operating on a frequency close to 5.405 GHz, is active somewhere along these lines [25]. Since an effective RFI pattern detection method is necessary for prior identification of RFI contaminated SAR images, the presented study focuses on the detection of RFI patterns (generated from powerful sources) which appear in publicly available Sentinel-1 satellite datasets using U-Net-like machine learning Convolutional Neural Network (CNN) algorithm.

The network used in the study is a U-Net-like architecture which is not exactly similar to the U-Net architecture. The model architecture is taken from the Keras official website (https://keras.io/). The architecture was originally applied for the segmentation of "Oxford Pets dataset". In the presented study this architecture is applied for the segmentation of RFI patterns which appear in publicly available Sentinel-1 satellite datasets. The CNN architecture used in the presented study is shown in figure 5.

Study Area and Datasets

The openly accessible Sentinel-1 GRD image, which is selected for the study is acquired over the North-West shoreline of UAE covering Dubai and Abu Dhabi as shown in figure 1. The image covers the range of latitude and longitude from 26.383N to 24.453N and 53.664E to 56.496E respectively. More than 60% of the study area is the ocean and the rest is land. The study area is selected with the help of the

"5Ghz Interference Locator" Google Earth Engine (GGE) application [26] by visualizing the RFI patterns over the area. The data properties of the Sentinel-1 image such as product type, product name, acquisition mode, antenna pointing direction, and flight direction are listed in table 1.

Table 1. Data properties of the Sentinel-1 image used for the study.

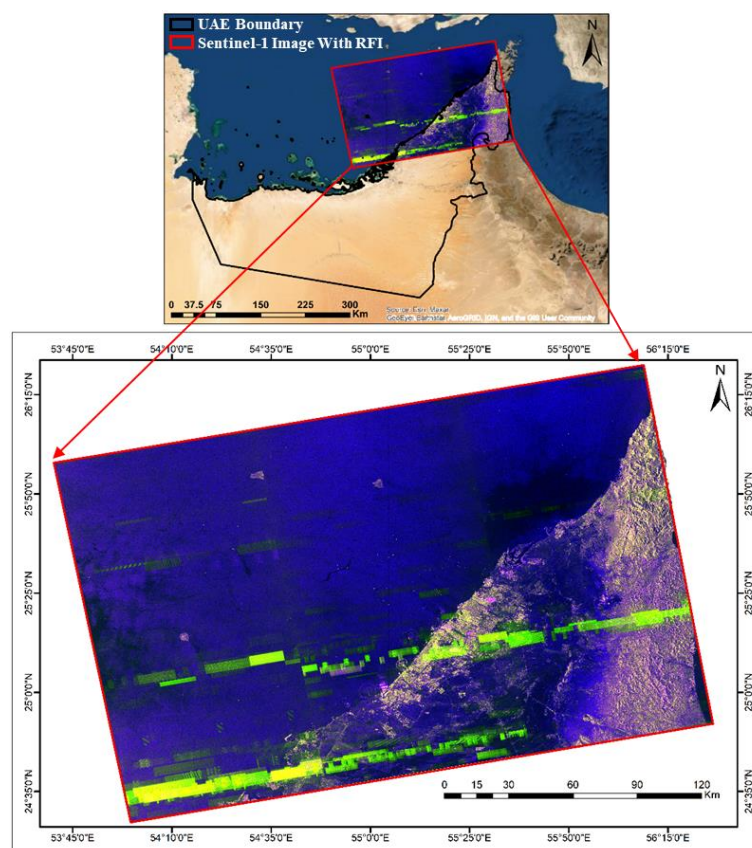| Sentinel-1 Image Data Properties	
Product Name	S1A_IW_GRDH_1SDV_20200527T142453_ 20200527T142518_032752_03CB42_DDD7
Product Type	GRD
Mission	Sentinel-1A
Antenna Pointing	Right
Acquisition Mode	IW
Pass	Ascending

Figure 1. Location of the study area with the RFI contaminated Sentinel-1 image.

Methodology

The methodology adopted for the study is shown in figure 2. The '5Ghz Interference Locator' GGE application has been utilized for the selection of the study area. which helps in providing the geolocations of potential sites on the ground where RFIs associated with the frequency bands near to 5 GHz are taking place. This application exploits ascending and descending pass images of Sentinel-1 constellation and provide a user-friendly online Graphical User Interface (GUI) for the visualization of RFI contaminated regions due to any possible reason. Since the Sentinel-1 image covers the Jabel Ali Port, therefore, maritime radar operating on the same frequency as of the Sentinel-1 radar may be the potential source of the appearance of RFI in the image acquired over this region. Most of the Sentinel-1 images acquired over this region are severely affected with RFI as examined using the "5Ghz Interference Locator" GGE

application. The RFI patterns over the study area as observed using the '5Ghz Interference Locator' GGE application are shown in figure 3. The RFI patterns for ascending and descending satellite passes are visible with two different colours making a cross sign with each other. According to a web article [25], the geo-location of the source of the RFI overlaps with the cross point of these patterns as shown in figure 3. These patterns are perpendicular to the corresponding satellite orbit trajectory.
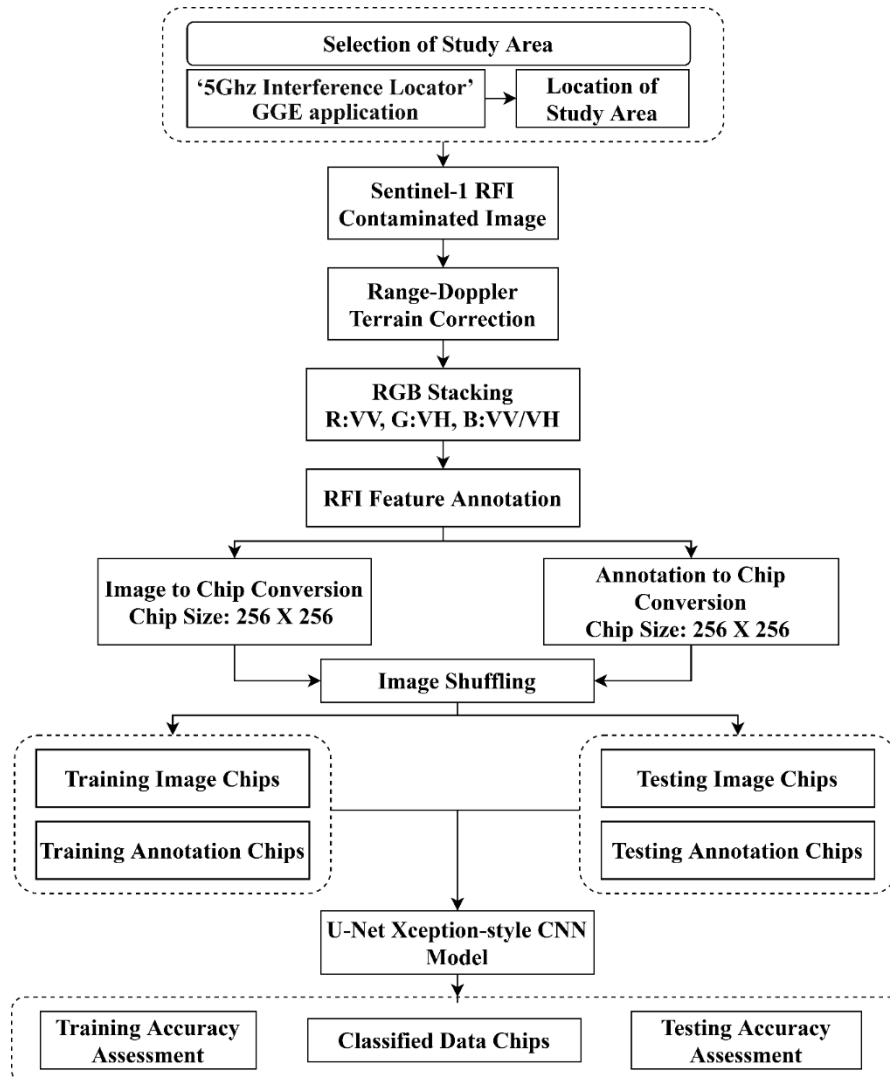

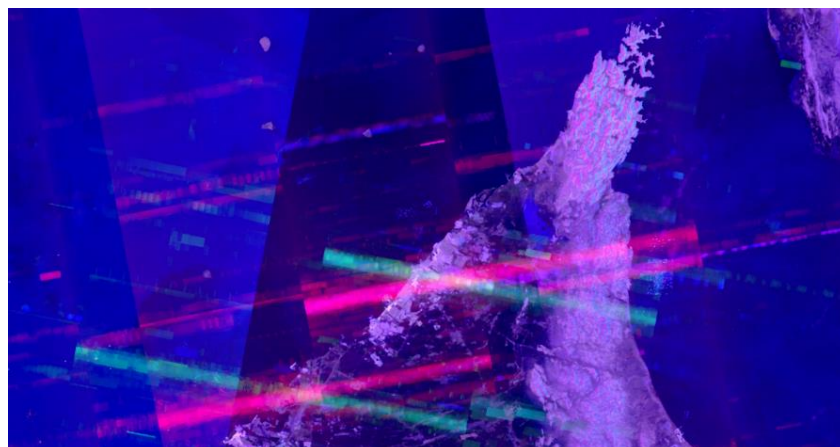*Figure 2. Flow chart for the methodology adopted in the presented study.*

Figure 3. The RFI patterns over the study are as observed from the '5Ghz Interference Locator' GGE application.

Data Pre-processing

The dual-band (VV- & VH-band) Sentinel-1A image of the selected study area was georeferenced (terrain corrected) with the help of "Range-Doppler Terrain Correction" toolbox available in the Sentinel Application Platform (SNAP) software of version 6.0. To avail the full information of all the bands, present in the data, an RGB stack (Red: VV-band, Green: VH-band, and Blue: VV/VH-band) was generated and exported in ".tif" format.

The ArcGIS Pro is the latest professional desktop Geographic information system (GIS) software from Esri. The software consists of toolboxes that support for data preparation and management for deep learning. The "Training Sample Manager" available in "Image Classification" toolbox of this software is used for the RFI feature annotation. Since the input and output of image segmentation model should be in a raster format for the training run, therefore, "Feature to Raster" function in ArcGIS Pro has been used to convert the labelled vector data from feature (vector) class format to raster format. The sentinel-1 image has a large swath width (250km) [27] and they cannot be fed directly to the model, therefore, the Sentinel-1 GRD image and corresponding labelled raster data (RFI annotation) were converted to smaller images (chips) by using "Export Training Data for Deep Learning" toolbox in ArcGIS Pro. The annotation raster chips consist of binary (0 or 1) pixel values. The pixels with value 1 and 0, represents the RFI features and background respectively as shown in figure 4. This tool allows choosing the size of each chip as well as a stride in X and Y axes. In this presented study, the chip size of 256 and stride size 0 along X and Y axes has been chosen. All the chips corresponding to the image raster and annotation raster were exported in ".png" format. A total of 2575 pair of image raster chips and corresponding annotation raster chips were exported. Some of the image chips and their corresponding annotation raster chips are shown in figure 4.
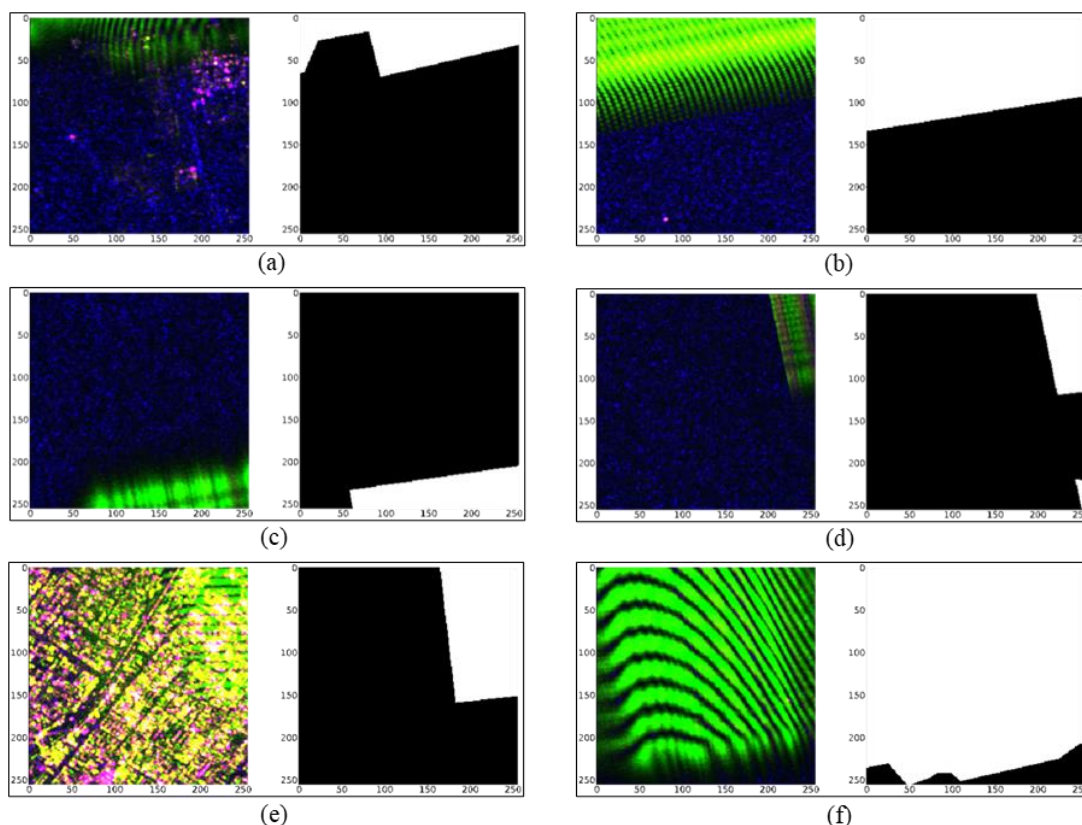

Figure 4. *The visual representation of Sentinel-1 RGB image chips of image size 256X256 and corresponding RFI feature annotation chips. (a), (b), (c), (d), (e), and (f) represents the 6 different pairs of Sentinel-1 RGB image chip (left) and corresponding RFI feature annotation chip (right).*

CNN Architecture and Specifications

Out of 2575 pairs of image raster chips and corresponding annotation raster chips, 1000 pairs were kept for the testing purpose of the U-Net-Like CNN model and rest were used for the training purpose. Optimizers are a crucial part of the neural network and the understanding of how they work helps to choose which one to use for the application. The "RMSprop" optimizer is used in the CNN model utilized for the presented study. It is an adaptive learning rate method and a well-known algorithm for mini-batch learning. It is a mini-batch version of "rprop" optimizer [28]. The central idea of RMSprop is to keep the moving average of the squared gradients for each weight and then divide the gradient by square root the mean square [28], which is why it is called RMSprop (Root Mean Square). RMSprop is a good and fast optimizer. It is one of the most popular optimization algorithms used in deep learning since its popularity is only surpassed by Adam.

In the presented study, the sparse categorical cross-entropy loss function is applied in the model. It computes the cross-entropy loss between the labels and predictions. This cross-entropy loss function is suggested to use when there are two or more label classes. The labelled raster datasets consist of two classes namely '0' and '1'. The '0' and '1' classes represent the non-RFI pixels and the RFI pixels in the image chips respectively. Softmax is the only activation function recommended to use with the categorical cross-entropy loss function.
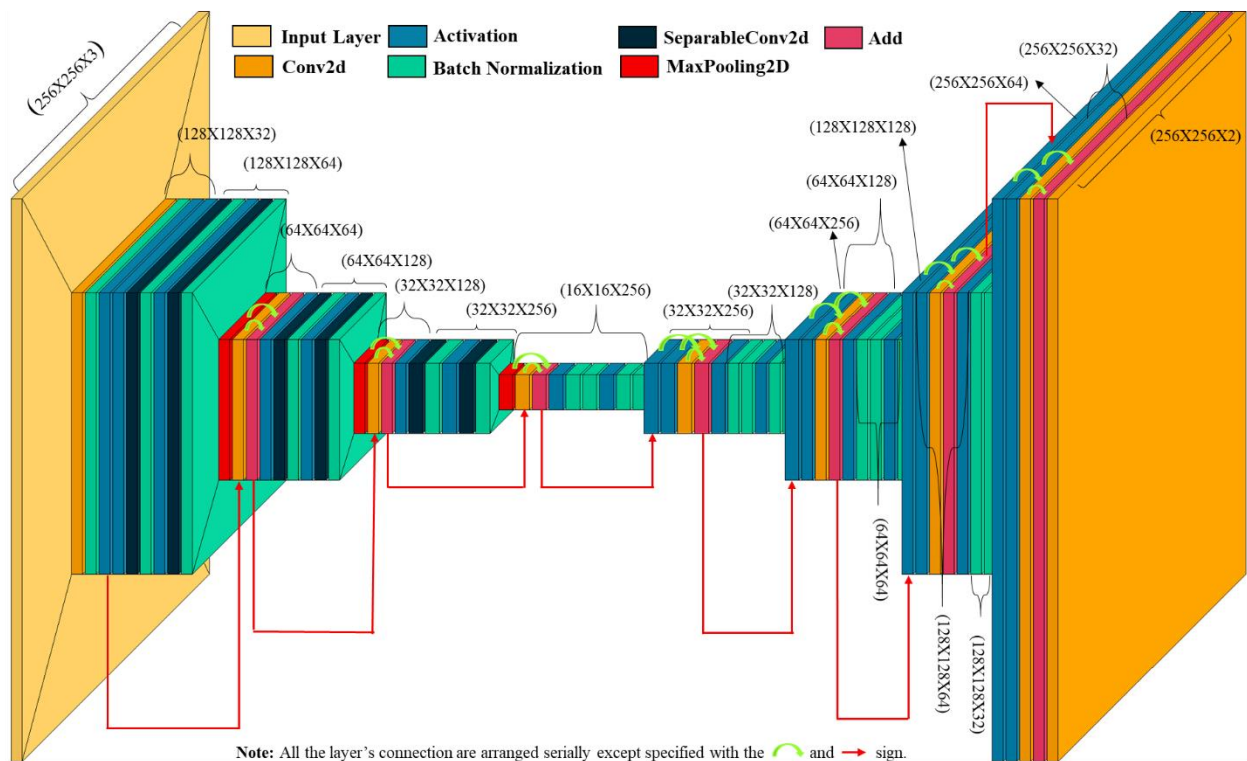

Figure 5. *Visual representation of CNN model architecture used in the study.*

Results and Discussion

The model was trained on 1575 pairs of image and annotation raster chips with 40 epochs. The training loss, validation loss, training accuracy, and validation accuracy values achieved on 40th epoch were found to be 0.0043, 0.0410, 0.9984, and 0.9921 respectively as shown in figure 8 and 9. Since the U-Net-Like CNN architecture is well-known for the better performance on a fewer number of input training datasets, the model performance is observed to be good with 1575 input training data chips. The

corresponding pixels of input RFI mask chips and the predicted mask chips were compared and the overall accuracy of 0.92 was achieved. The classification report with precision, recall, f1-score and support for RFI (pixel value 1) and background class (pixel value 0) for the validation input masks and corresponding predicted masks is shown in figure 7. The precision, recall, and f1-score for Background class were found to be 0.94, 0.98, and 0.96 respectively. Whereas, the precision, recall, and f1-score for RFI class were found to be 0.78, 0.53, and 0.63 respectively.

The input image chips used for the validation and their corresponding RFI masks and predicted RFI masks are shown in figure 6. It is evident from the CNN model prediction as shown in figure 6 that presented CNN model performed better for the prediction of the sharp edges of RFI patterns. Along with the combinations of RGB pixel values corresponding to the RFI feature in the image chips, the model is also capable of capturing the texture information of the RFI features.
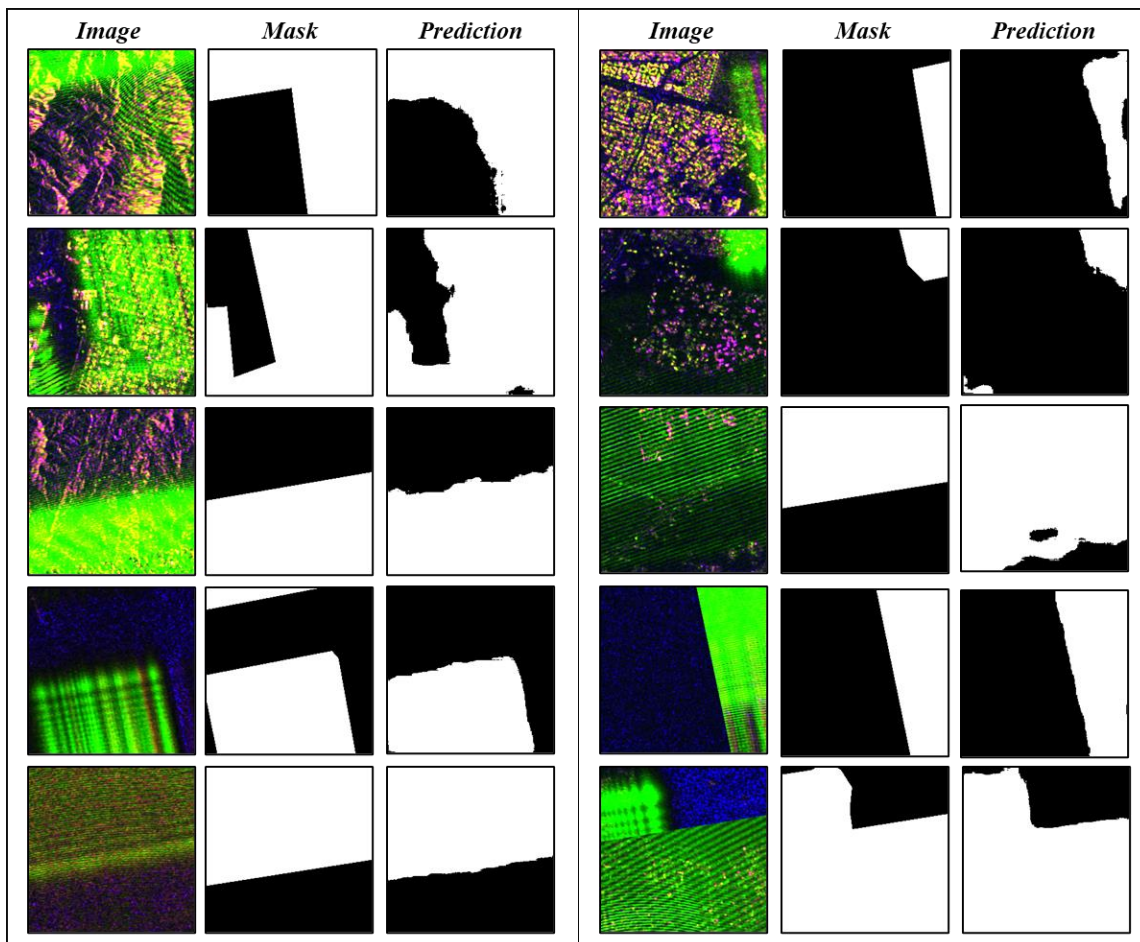

Figure 6. *Examples of few input validation images with corresponding given RFI masks and model predicted RFI masks.*

	precision	recall	f1-score	support
0	0.94	0.98	0.96	57475072
1	0.78	0.53	0.63	8060928
accuracy			0.92	65536000
macro avg	0.86	0.75	0.79	65536000
weighted avg	0.92	0.92	0.92	65536000

Figure 7. *The classification report with precision, recall, f1-score and support for RFI (pixel value 1) and background class (pixel value 0) for the validation input masks and corresponding predicted masks.*
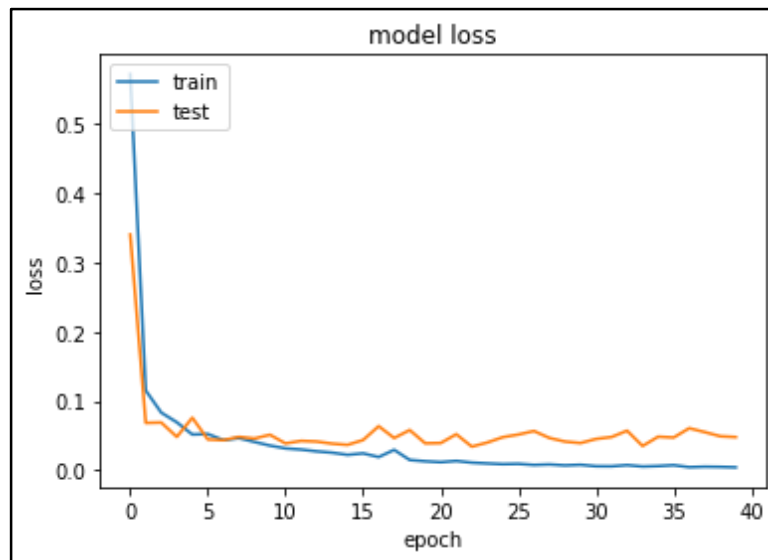
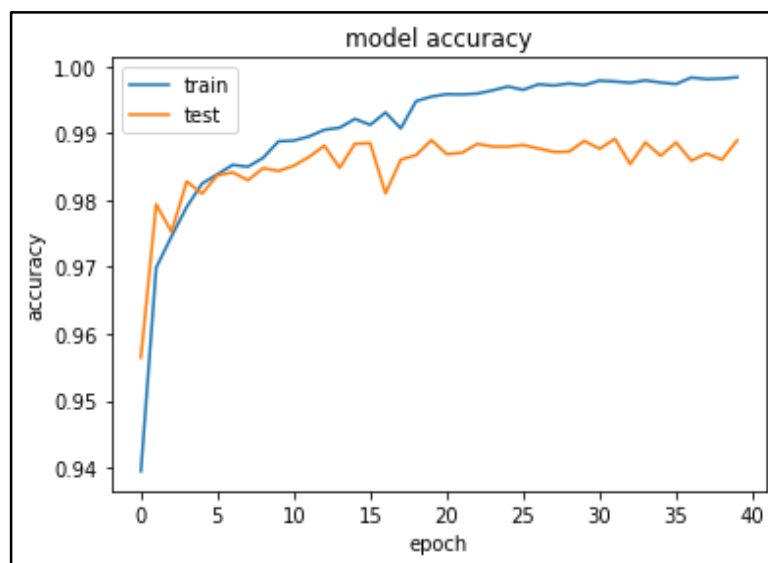**Figure 8.** *The training and validation loss of model with each epoch.*

Figure 9. *The training and validation accuracy of the model with each epoch.*

Conclusions

The automatic identification of RFI contaminated Sentinel-1 images is a prior step while processing a huge number of Sentinel-1data images for various land and ocean applications. The presented study suggests that machine learning U-Net-Like CNN architecture model can be effectively used for the prior identification of RFI contaminated Sentinel-1 images in an automatic way. Along with the presence of RFI patterns in the image, the information about the geo-locations of these RFI patterns can also be effectively identified with the help of machine learning U-Net-Like CNN architecture model. The performance of the model can be further improved by increasing the number of input training data chips containing complexity and high variability of the RFI features. Since the Sentinel-1 "Quick Look" RGB images, accessible from https://scihub.copernicus.eu/, are resampled to the lower resolution and smaller in size, the presented model can also be trained on these images for the quick prediction of RFI patterns in the images.

References

[1]   A. Moreira, P. Prats-Iraola, M. Younis, G. Krieger, I. Hajnsek, and K. P. Papathanassiou, "A tutorial on synthetic aperture radar," *IEEE Geosci. Remote Sens. Mag.*, vol. 1, no. 1, pp. 6–43, 2013, doi: 10.1109/MGRS.2013.2248301.

[2]   J. Dudczyk, A. Kawalec, and J. Cyrek, "Applying the distance and similarity functions to radar signals identification," 2008, doi: 10.1109/IRS.2008.4585771.

[3]   J. Dudczyk and A. Kawalec, "Optimizing the minimum cost flow algorithm for the phase unwrapping process in SAR radar," *Bull. Polish Acad. Sci. Tech. Sci.*, vol. 62, no. 3, pp. 511–516, Sep. 2014, doi: 10.2478/bpasts-2014-0055.

[4]   W. Fan *et al.*, "Interference Mitigation for Synthetic Aperture Radar Based on Deep Residual Network," *Remote Sens.*, vol. 11, no. 14, p. 1654, Jul. 2019, doi: 10.3390/rs11141654.

[5]   A. Reigber *et al.*, "Very-high-resolution airborne synthetic aperture radar imaging: Signal processing and applications," *Proc. IEEE*, vol. 101, no. 3, pp. 759–783, 2013, doi: 10.1109/JPROC.2012.2220511.

[6]   F. Bovenga, "Special issue 'synthetic aperture radar (SAR) techniques and applications,'" *Sensors (Switzerland)*, vol. 20, no. 7. MDPI AG, Apr. 01, 2020, doi: 10.3390/s20071851.

[7]   W. Alpers, B. Holt, and K. Zeng, "Oil spill detection by imaging radars: Challenges and pitfalls," *Remote Sens. Environ.*, vol. 201, pp. 133–147, Nov. 2017, doi: 10.1016/j.rse.2017.09.002.

[8]   H. Greidanus, "Satellite imaging for maritime surveillance of the European seas," in *Remote Sensing of the European Seas*, Springer Netherlands, 2008, pp. 343–358.

[9]   V. Barale and M. Gade, *Remote sensing of the European seas*. Springer Netherlands, 2008.

[10]   R. Gens, "Oceanographic applications of SAR remote sensing," *GIScience and Remote Sensing*, vol. 45, no. 3. Taylor & Francis Group , pp. 275–305, Jul. 2008, doi: 10.2747/1548-1603.45.3.275.

[11]   W. Dierking and T. Busche, "Sea ice monitoring by L-band SAR: An assessment based on literature and comparisons of JERS-1 and ERS-1 imagery," in *IEEE Transactions on Geoscience and Remote Sensing*, Apr. 2006, vol. 44, no. 4, pp. 957–970, doi: 10.1109/TGRS.2005.861745.

[12]   V. Kerbaol and F. Collard, "SAR-derived coastal and marine applications: From research to operational products," *IEEE J. Ocean. Eng.*, vol. 30, no. 3, pp. 472–486, Jul. 2005, doi: 10.1109/JOE.2005.857505.

[13]   H. Balzter, "Forest mapping and monitoring with interferometric synthetic aperture radar (InSAR)," *Prog. Phys. Geogr. Earth Environ.*, vol. 25, no. 2, pp. 159–177, Jun. 2001, doi: 10.1177/030913330102500201.

[14]   M. Craig Dobson, F. T. Ulaby, and L. E. Pierce, "Land-cover classification and estimation of terrain attributes using synthetic aperture radar," *Remote Sens. Environ.*, vol. 51, no. 1, pp. 199–214, Jan. 1995, doi: 10.1016/0034-4257(94)00075-X.

[15]   H. McNairn and J. Shang, "A review of multitemporal synthetic aperture radar (SAR) for crop monitoring," in *Remote Sensing and Digital Image Processing*, vol. 20, Springer International Publishing, 2016, pp. 317–340.

[16]   P. W. M. Souza-Filho and W. R. Paradella, "Use of synthetic aperture radar for recognition of Coastal Geomorphological Features, land-use assessment and shoreline changes in Bragança coast, Pará, Northern Brazil," *An. Acad. Bras. Cienc.*, vol. 75, no. 3, pp. 341–356, 2003, doi: 10.1590/S0001-37652003000300007.

[17]   N. Kussul, A. Shelestov, and S. Skakun, "Flood Monitoring from SAR Data," *NATO Sci. Peace Secur. Ser. C Environ. Secur.*, vol. 97, pp. 19–29, 2011, doi: 10.1007/978-90-481-9618-0_3.

[18]   A. Geymen, "Digital elevation model (DEM) generation using the SAR interferometry technique," *Arab. J. Geosci.*, vol. 7, no. 2, pp. 827–837, Feb. 2014, doi: 10.1007/s12517-012-0811-3.

[19]   D. Raucoules, C. Colesanti, and C. Carnec, "Use of SAR interferometry for detecting and assessing ground subsidence," *Comptes Rendus - Geosci.*, vol. 339, no. 5, pp. 289–302, Apr. 2007, doi: 10.1016/j.crte.2007.02.002.

[20]   T. Bollian, B. Osmanoglu, R. Rincon, S. K. Lee, and T. Fatoyinbo, "Adaptive antenna pattern notching of interference in synthetic aperture radar data using digital beamforming," *Remote Sens.*, vol. 11, no. 11, p. 1346, Jun. 2019, doi: 10.3390/rs11111346.

[21]   *A strategy for active remote sensing amid increased demand for radio spectrum*. National Academies Press, 2015.

[22]   A. Chojka, P. Artiemjew, and J. Rapiński, "RFI artefacts detection in sentinel-1 level-1 SLC data based on image processing techniques," *Sensors (Switzerland)*, vol. 20, no. 10, May 2020, doi: 10.3390/s20102919.

[23]   M. Tao, F. Zhou, and Z. Zhang, "Wideband Interference Mitigation in High-Resolution Airborne Synthetic Aperture Radar Data," *IEEE Trans. Geosci. Remote Sens.*, vol. 54, no. 1, pp. 74–87, Jan. 2016, doi: 10.1109/TGRS.2015.2450754.

[24]   K. Schmidt, M. Schwerdt, N. Miranda, and J. Reimann, "Radiometric Comparison within the Sentinel-1 SAR Constellation over a Wide Backscatter Range," *Remote Sens.*, vol. 12, no. 5, p. 854, Mar. 2020, doi: 10.3390/rs12050854.

[25]   "SENTINEL-1   C-SAR   interference   analysis.   Intro   -   OSINTEditor." https://www.osinteditor.com/resources/sentinel-1-c-sar-interference-analysis-intro/   (accessed Nov. 02, 2020).

[26]   "5Ghz Interference Tracker." https://orbtwz.users.earthengine.app/view/radarinterferencetracker (accessed Nov. 02, 2020).

[27]   T. Nagler, H. Rott, M. Hetzenecker, J. Wuite, and P. Potin, "The Sentinel-1 mission: New opportunities for ice sheet observations," *Remote Sens.*, vol. 7, no. 7, pp. 9371–9389, Jul. 2015, doi: 10.3390/rs70709371.

[28]   G. Hinton, N. Srivastava, and K. Swersky, "Neural Networks for Machine Learning Lecture 6a Overview of mini-‐-batch gradient descent."